# Evaluation of Pore Volume, Connectivity and Clogging of Previous Concrete Reactive Barrier in Treatment of Acid Mine Drainage

**Stephen O. Ekolu**
Nelson Mandela University
**Fitsum Solomon** ( Fitsummoa@gmail.com )
University of Johannesburg Faculty of Engineering and Built Environment
**Frikkie de Beer**
Nuclear Technolgy Division, NECSA
**Louisette Bitandi**
University of Johannesburg Faculty of Engineering and Built Environment
**Rais N. Kilula**
University of Johannesburg Faculty of Engineering and Built Environment
**Khaya T. Maseko**
University of Johannesburg Faculty of Engineering and Built Environment
**Fatty G. Mahlangu**
University of Johannesburg Faculty of Engineering and Built Environment

**Research Article**

**Keywords:** Pervious concrete, pore volume, permeability, clogging, connectivity, image analysis, X - ray micro - computed tomography.

**Posted Date:** October 12th, 2021

**DOI:** https://doi.org/10.21203/rs.3.rs-775639/v1

## Abstract

It has recently been shown that pervious concrete is a promising, effective technology as permeable reactive barrier for treatment of acid mine drainage (AMD). However, pore clogging also occurs simultaneously during AMD treatment. In the present study, mixtures of pervious concrete were made and used in a column experiment during which pore clogging occurred in the samples. Pore volume, connectivity and other parameters of pervious concrete were evaluated using five (5) different methods comprising the volumetric method (VM), linear – traverse method (LTM), image analysis (IA), falling head permeability test and X - ray micro - computed tomography.

It was found that pervious concrete effectively removed from AMD, about 90 to 99% of various heavy metals including Al, Fe, Zn, Mn and Mg. Cr concentration significantly increased in the treated effluent, owing to leaching from cementitious materials used in mixtures. The VM and LTM gave statistically similar pore volume results, while IA's values were 20 to 30% higher than those of the conventional methods. The falling head permeability test and IA were found to be effective in quantifying pore clogging effects. Pervious concrete exhibited high pore connectivity of 95.0 to 99.7%, which underlies its efficacious hydraulic conductivity.


## 1. Introduction

Pervious concrete is purposely made using single - size aggregate along with other mix ingredients, incorporated in proportions that give high porosity levels of 20 to 30%. At this level of porosity, the pore network of pervious concrete is highly interconnected with large pores of 2 to 8 mm sizes, that allow free flow of water (Kia et al., 2017; Ekolu et al., 2014). Ekolu et al. (2016) measured a wide range of pervious concrete mixtures and obtained water permeability values of 2 to 20 mm/s. Other researches (Zhong et al., 2018) have reported permeability values of 2 to 8 mm/s.

## 1.1 Pervious concrete applications

The main engineering applications of pervious concrete technology are stormwater management and innovative treatment of polluted water such as acid mine drainage (AMD), wastewater etc. Recent researches have shown that pervious concrete is effective as a permeable reactive barrier (PRBs) for treatment of AMD (Majersky, 2009; Park and Tia, 2004; Ekolu et al., 2014; Ekolu and Bitandi, 2018; Holmes et al., 2017). PRB technology is considered to be a relatively more sustainable, cost – effective passive treatment system for AMD, compared to the conventional active pump and treat system (Obiri-Nyarko et al., 2014; Thiruvenkatachari et al., 2008; Morrison et al., 2003; Gavaskar, 1999; Gavaskar et al., 1998; Mulligan et al., 2001; Ekolu et al., 2014; 2016; Muthu et al., 2018; Bartzas and Komnitsas, 2010).

In the industry, pervious concrete is more commonly employed as pavement material for construction of parking lots, driveways, sidewalks and low - volume traffic roads. Pervious concrete pavements (PCPs) are typically 75 to 300 mm thick. During a rain event, surface water percolates through the PCP to the soil beneath, thereby reducing surface run – off by 50 to 100% (Kia et al., 2017). Water flow through PCP typically exceeds 0.34 cm/s, which is well above the recommended minimum infiltration rate of 0.162 cm/s (Tennis et al., 2004; Kia et al., 2017).

Interestingly, as run - off percolates through the porous pavement, pervious concrete tends to attenuate suspended solids, removes heavy metals such as As, Fe, Cu, Al, Zn, P, Pb etc., and decreases hydrocarbons including motor oil, grease etc. (Kevern et al., 2008; Kia et al., 2017; Brown, 2013; Collins et al., 2008; Pratt et al., 1995; Lucke and Beecham, 2011; Pagotto et al., 2000; Sañudo-Fontaneda et al., 2014; Ong et al., 2016; Zhong et al., 2018).

However, researches have shown that clogging is a major threat to field application of pervious concrete technology. Physical accumulation of debris within pores of pervious concrete, severely reduces water infiltration rate, thereby adversely affecting the system's hydraulic performance (Kia et al., 2017). Also, blockage of pores due to clogging compromises the pavement's freeze – thaw resistance, leading to early failure and a shorter service lifespan. Several of the reported failures in field PCPs, are attributed to clogging (Radlinska et al., 2012; Kia et al., 2017).

Pore volume and pore size distribution (PSD) are the two important parameters that underlie hydraulic conductivity as a property of pervious concrete. Pore volume consists of *isolated* pores and *interconnected* pores. It is the volume of interconnected pores i.e. *effective porosity*, that determines water flow transmission through pervious concrete (Zhong et al., 2018).

## 1.2 Study objectives

Following earlier pioneering works (Ekolu et al., 2014; 2018), the present study was conducted to affirm pervious concrete's efficacy as an effective technology for AMD treatment, while focussing on investigation of pore parameters responsible for its efficacious hydraulic conductivity, along with some limitations such as chemical clogging. As such, this research focussed on evaluation of pore volume, connectivity and clogging of pervious concrete in AMD treatment. Among key objectives, was identification of the techniques capable of effectively quantifying pore clogging effects. Accordingly, the foregoing parameters were measured using five (5) different conventional methods and advanced techniques comprising:- the volumetric method (VM) (ASTM C1754, 2012; Montes et al., 2005) and linear – traverse method (LTM) (ASTM C457, 2016) employed for pore volume measurement, image analysis (IA) used to determine PSD, the falling head permeability test conducted to measure hydraulic conductivity as an indirect indicator of pore connectivity, while X - ray micro - computed tomography (microCT) was done to examine and quantify pore connectivity. Statistical analysis was conducted to compare results obtained using the different porosity measurement methods.

# 2. Column Experiment And Results

## 2.1 Pervious concrete mixtures

Ordinary Portland cement CEM I 52.5 N with or without 30% fly ash (FA), was used to prepare various pervious concrete mixtures at water /cementitious ratio (w/cm) of 0.25, 0.27 or 0.28. CEM I – pervious concrete mixtures were prepared with aggregates of different types and sizes comprising 6.7 mm granite stone (G6.7), 9.5 mm granite stone (G9.5), 13.2 mm granite stone (G13.2), 9.5 mm andesite stone (A9.5), 6.7 mm dolomite stone (D6.7), 9.5 mm dolomite stone (D9.5) and 6.7 mm shale stone (S6.7). The mixture G6.7FA contained 30% FA as partial CEM I replacement i.e. 30FA – pervious concrete. Table 1 gives a full range of the various mix design proportions used. Cubes of 100 mm size were cast and cured in water for 28 days. Compositions of the cement and FA materials used, are already given in Ekolu and Bitandi (2018).

## 2.2 Experimental set – up

Figure 1 gives experimental set – up of the 100 x 100 x 650 mm height square columns of pervious concrete. The AMD used in the column experiment was obtained from an abandoned coal mine, designated as TDB. Composition of the raw TDB is given in Table 1. The column experiment involved continuous pumping of AMD influent at a constant flow rate of 1.0 mL/min, from the bottom ends of columns upwards against gravity. Other details of the experimental set - up are given in Ekolu and Bitandi (2018). It can be seen in Fig. 1b that sludge deposition within the column, occurred during AMD treatment. Build – up of the brownish sludge clogging observed in Fig. 1b, initiated at the bottom and progressed upwards the column height. Following long – term continuous pumping of AMD through the column, clogging eventually advanced throughout the full height, as seen in Fig. 1c. The observed clogging is attributed to formation of heavy metal precipitates, seen as sludge deposition within pervious concrete pores. In Table 1, the samples assigned the 'C' designation i.e. 6.7C, 9.5C and 13.2C, indicate mixtures that were exposed to AMD for at least 90 – days, during which some pore clogging occurred.

Table 1
Pervious concrete mixtures used.

| Ingredients | Mixture quantities | | | | | | | |
|---|---|---|---|---|---|---|---|---|
| *Aggregate type and size | D9.5 | D6.7 | A9.5 | *G6.7 | G6.7FA | $G9.5 /G9.5C | G13.2 /G13.2C | S6.7 /S6.7C |
| Water /cement ratio (w/c) | 0.27 | 0.27 | 0.27 | 0.27 | 0.27 | 0.28 | 0.25 | 0.25 |
| Cement (kg) | 4.7 | 4.7 | 4.7 | 4.7 | 3.3 | 2.3 | 3.7 | 3.3 |
| 30% fly ash, FA (kg) | | | | | 1.4 | | 1.0 | 1.4 |
| Aggregates (kg) | 18.9 | 18.9 | 18.9 | 18.9 | 18.9 | 18.9 | 18.9 | 18.9 |
| Water (kg) | 1.3 | 1.3 | 1.3 | 1.3 | 1.3 | 1.3 | 1.3 | 1.3 |
| Chryso PREMIA 310 (mls) | 78 | 48 | 26 | 48 | 48 | 60 | 86 | 92 |

*Aggregate type: D – dolomite, A – andesite, G – granite, S – shale.

$G9.5 – Plain pervious concrete samples made with 9.5 mm granite aggregate, G9.5C – Pervious concrete samples made with 9.5 mm granite aggregate and exposed to acid mine drainage for at least 90 days, during which pore clogging occurred, *G6.7FA – Pervious concrete containing 30% fly ash and made with 6.7 mm granite aggregate.

## 2.3. Results of acid mine drainage treatment

Pore clogging may potentially affect the pervious concrete's efficacy of treating AMD. This aspect of study was evaluated by:- (a) comparing the mass of AMD influent versus that of effluent, (b) evaluating contaminant removal efficiency (RE), and (c) assessing the quality of treated AMD effluent over the duration of study. RE was calculated using Eq. (1), as the percentage amount of heavy metals removed following AMD treatment.

$$\mathrm{RE}\ (\%) = \frac{C_o - C_e}{C_o} x\,100 \qquad (1)$$

where $C_o$ and $C_e$ are the initial and equilibrium concentrations (mg/L) of contaminant(s) before and after AMD treatment, respectively.

It can be seen in Fig. 2 that mass values of effluent were lower than corresponding values of the influent. The observed reduction in mass values of the effluent is attributed to removal of heavy metal contaminants from AMD, resulting in pore clogging due to sludge deposition (Fig. 1b,c). Intense pore clogging of pervious concrete may adversely affect both the concrete's hydraulic conductivity and contaminant RE. It is evident in Fig. 2 that RE decreased rapidly within the first two weeks of continuous AMD treatment, eventually attaining steady – state values as low as about 20% and 10% for 30FA - and CEM1 - pervious concretes, respectively. The observed rapid reduction in RE at early stages of AMD treatment, is attributed to armouring of reacted cement and FA particle surfaces, owing to deposition of metal precipitates at or close to reaction sites.

Interestingly, the quality of treated water remained similar before and after significant clogging (Fig. 1b) had occurred, following 90 days of continuously using the pervious concrete column to treat AMD. It can be seen in Table 2 that the quality of treated water effluent at 90 days, remained generally similar to the quality achieved at the earlier stages within 7 days of continuously pumping AMD through the column. The pH level of treated water was consistently about 10, which is significantly high relative to 2.99 of raw TDB. It is evident that pervious concrete effectively removed the pH – dependent elements including Al, Fe, Zn, Mn and Mg from AMD, giving high RE values of 90 to 99% (Table 2). However, only minor reduction in $SO_4$ concentration was observed, while the alkali metals comprising Na, K or Ca increased slightly in the treated effluent (Table 2). It is notable that Cr concentration in treated AMD effluent, increased significantly relative to that of raw TDB. The observed higher Cr concentration in treated effluent, is attributed to leaching of the hazardous element from cementitious materials comprising the CEM I and FA

used in pervious concrete mixtures. Typical concentrations of total chromium $Cr_2O_3$ in South African CEM I and FA are 102 and 200 ppm, of which 30 to 80% is the partially leacheable hazardous Cr(VI) (Sawyer et al., 2012; Potgieter et al., 2003).

Table 2
Water quality following treatment of acid mine drainage using 30FA - pervious concrete.

| Element | | Al (mg/L) | Fe (mg/L) | Zn (mg/L) | Mn (mg/L) | Mg (mg/L) | $SO_4$ (mg/L) | Ca (mg/L) | Na (mg/L) | K (mg/L) | Cr (mg/L) |
|---|---|---|---|---|---|---|---|---|---|---|---|
| Raw TDB | pH = 2.99 | 6.04 | 4.48 | 0.978 | 14 | 223 | 6 718 | 383 | 2215 | 40 | < 0.025 |
| Water quality at 7 days of continuous AMD treatment* | pH = 10.5 | < 0.100 | 0.180 | < 0.025 | 0.080 | 2.0 | 4852 | 537 | 2237 | 156 | 0.222 |
| Water quality and RE at 90 days of continuous AMD treatment* | pH = 10 | 0.113 | < 0.025 | < 0.025 | < 0.025 | 30 | 5417 | 440 | 2525 | 57 | 0.053 |
| | RE (%) | 98.1 | 99.4 | 97.4 | 99.8 | 86.5 | 19.4 | -14.9 | -14.0 | -42.5 | -112.0 |

*Water quality produced following 7 or 90 days of continuously pumping acid mine drainage (AMD) through the 30FA - pervious concrete column; TDB – raw AMD.

## 3. Measurement Of Pore Characteristics, Parameters And Clogging

The pervious concrete cube samples were drilled to extract cores of 70 dia. x 100 mm height. Some cores were cut into 70 dia x 35 mm thick discs, which were then used for determination of pore volume results or PSDs, as per the VM, LTM and IA procedures.

The falling head permeability test was done on various pervious concrete cores, while a limited number of core specimens were analysed using X – ray microCT to quantify pore connectivity. Figure 3 shows cube samples along with cores and disc specimens that were prepared for conducting the various tests.

# 3.1 Tests and measurement methods

# 3.1.1 Measurement of pore volume and pore size distribution

Flat surfaces of the 70 dia. x 35 mm thick disc specimens, were polished using successively finer abrasives to produce a satisfactorily smooth surface finish. Pore volume and PSD tests were done on the disc specimens, employing all three different methods comprising the VM, LTM and IA. It may be recalled that the VM and LTM only measure pore volume, while IA determines PSD.

*(a) Volumetric method*

The VM's standard procedure given in ASTM C1754 (2012) (Montes et al., 2005) was used to determine pore volume of pervious concrete, based on low drying temperature. The procedure involved oven - drying the 70 dia. x 35 mm thick disc specimens for 24 hours at 40$^{o}$C, followed by weighing in air ($W_D$) and in water (Ws). Pore volume ($P_v$) was calculated using Eq. (2).

Pore volume (%) = $[1-((W_D - W_S)/ \rho_w)/ V_T] \times 100$ (2)

where $W_D$ - oven dry weight (g), $W_S$ - submerged weight (g), $\rho_w$ - density of water (g/cm$^3$), $V_T$ - total volume of specimen (cm$^3$).

*(b) Linear - traverse method*

The LTM procedure given in ASTM C457 (2016) is a standard microscopical technique for determining the void content of normal concrete. In the present study, the method was innovatively employed to determine pore volume of pervious concrete. The measurement procedure involved drawing parallel lines across flat surfaces of disc specimens. The total sum of line lengths traversing across void components at the disc surface ($T_a$), is expressed as a proportion of the total sum of all line lengths drawn across the surface ($T_t$). Figure 4 shows parallel lines spaced 2.5 mm apart, drawn across flat surfaces of disc specimens. For each specimen, $T_a$ and $T_t$ were determined then used to calculate void content ($P_{LT}$), as per Eq. (3).

$$\text{Void content } (\%) = \frac{\sum_1^n \text{Ta}_i}{T_t} \text{ x } 100 \quad (3)$$

where $Ta_i$ – length of a line traversing a void component (i), $T_t$ – total length of all lines traversing across the whole disc surface, n – total number of void components encountered across the disc surface.

*(c) Image analysis*

Upon completion of pore volume measurements done on disc specimens as per the VM and LTM, the same specimens were then prepared for IA. The IA preparation procedure involved coating the flat surfaces of disc specimens using white paint. After the coating had dried, painted surfaces of the specimens were scanned using a flatbed scanner to acquire processed images.

Figure 5 shows some representative scanned images of disc specimens. White areas of the binary (black /white) images indicate solid components, while the irregular black spots are pores. It can be seen in Fig. 5, that aggregate sizes significantly influence pore interconnectivity. As the aggregate size used in pervious concrete reduced, pore sizes correspondingly became more numerous and smaller in size (Fig. 5a of specimen G6.7). In contrast, use of larger aggregate sizes in pervious concrete led to fewer but larger pore sizes (Fig. 5b,c of specimens G9.5, G13.2). It is also evident that the pores within each specimen, are randomly distributed from small to larger sizes.

In the present study, the IA free software *Image J* which is freely available at http://rsbweb.nih.gov/ij/, was used to conduct PSD analysis (Ferreira and Rasband, 2012). Pore area is determined as *the number of pixels occupying a given pore space* x *area per pixel*. The calculated area of a pore is converted into a circle of an equivalent area. The circle's diameter is taken as the equivalent pore diameter. A histogram is then plotted for various pore sizes occurring across the surface, resulting in a cumulative frequency distribution curve of pore sizes i.e. the PSD curve. Threshold pore diameter is obtained as the pore size ($d_c$) taken at 50% proportion of the cumulative frequency distribution curve (Neithalath et al., 2010).

IA employs the underlying assumption that the fraction of pores determined based on 2D area analysis is equivalent to the 3D volume fraction. However, various researches (Diamond and Leeman, 1995; Eshel et al., 2004) have shown that this assumption may be responsible for the observed IA's overestimation of pore volume or PSD.

## 3.1.2 Permeability measurement

A falling - head permeameter shown in Fig. 6 was built in - house within the laboratory, in accordance with details given in Das (1988). The permeameter comprised a 450 mm long graduated cylinder of 72 mm inner dia., connected to a U – pipe fitted with a valve. The test set - up involved inserting a saturated core specimen inside a rubber tube of 65 mm dia., during which the tubing was circumferentially stretched to tightly hold the 70 mm dia. core against radial water flow. Clamps were used to attach the sample in position, as shown in Fig. 6. Water was added into the graduated cylinder until its level at both the cylinder and at the drain pipe, reached the same height, then the valve was closed. Afterwards, the graduated cylinder was filled with water up to the maximum height level of 350 mm. Each test run involved opening the valve and measuring the time (in seconds) taken for water to drain through the core specimen, from the initial hydraulic head ($h_1$) of 350 mm to the lower head ($h_2$) of 50 mm. Three test runs were done for each core specimen. Permeability was calculated using Eq. (4) (Das, 1988).

$$k = \frac{aL}{At} \ln\left(\frac{h_1}{h_2}\right) \quad (4)$$

where k - permeability (m/s), a - cross section area of the tube ($m^2$), L - height of the core sample (m), A – cross section area of the core sample ($m^2$), t - time taken for water level to drop from the height of $h_1$ to $h_2$ (seconds), $h_1$ - upper height level of water (m), $h_2$ - lower height level of water (m).

### 3.1.3 Pore connectivity determination

A limited set of core specimens were analysed using X – ray microCT to quantify pore volume, connected porosity, isolated porosity and pore connectivity. Of the methods employed in the present study, microCT was the only technique capable of directly quantifying pore connectivity, while also characterizing the spatial pore distribution features (du Plessis and Boshoff, 2019).

## 3.2 Discussion of measured pore parameters and clogging effects

### 3.2.1 Pore volume results

Figure 7 gives the pore volume results determined as per the VM, LTM and IA. It can be seen that the pore volume results obtained are within 16 to 30%, which is the typical range of porosity values for pervious concretes (Ekolu et al., 2016). The mixtures made with dolomite aggregate, gave pore volume results that were generally lower than the corresponding values obtained for the samples made with the other aggregate types.

It is also evident that the pervious concrete samples G9.5C, G13.2C and S6.7C, which had been used to treat AMD in turn giving rise to pore clogging, showed porosity values that were similar to those of the control samples (G9.5, G13.2, S6.7) that had not been exposed to AMD. These observations show that the VM and LTM were unable to determine pore clogging effects. It is known that clogging occurs as discrete blockages within small pores, forming bottlenecks inside an interconnected pore network. Such small discrete blockages are unlikely to significantly affect the bulk pore volume results determined using the conventional methods.

### 3.2.2 Pore size distribution results

IA was employed to determine the PSDs of pervious concretes, as shown in Fig. 8. It can be seen that the pore volume ($P_I$) results determined using IA, are generally within the range of 15 to 35%. These values are similar to the pore volume results that were determined using the VM and LTM (Sect. 3.2.1). The observed maximum pore sizes (*mps*) in the pervious concretes, were generally between 10 to 15 mm. Moreover, the *mps* values increased with corresponding increase in the aggregate sizes used to prepare the pervious concretes. These findings are consistent with the visual observations discussed in Sect. 3.1.1c, showing that pervious concretes made with larger aggregate sizes, depicted correspondingly greater *mps* values.

### 3.2.3 Statistical comparison of pore volume results

Figures 9 gives pairwise comparisons for the pore volume results comprising $P_v$, $P_{LT}$ and $P_I$, that were determined in accordance with the VM, LTM and IA, respectively. Evidently, $P_v$ and $P_{LT}$ show strong agreement with values lying along the line of equality (Fig. 9a). In the converse, $P_I$ results are consistently higher than the corresponding $P_v$ or $P_{LT}$ values, as seen in Fig. 9b,c. The tendency of IA to overestimate porosity values or PSDs, relative to those determined using conventional methods, is well - established (Diamond and Leeman, 1995). The assumption employed in IA, which considers the 2D area fraction of an irregularly shaped pore as equal to volume fraction of an equivalent pore sphere, is responsible for the method's tendency to overestimate porosity (Sect. 3.1.1c). It is known that a non - spherical particle measured across all orientations, gives a cross - sectional area that is larger than that of a sphere which has an equivalent volume as the particle (Eshel et al., 2004).

Statistical analysis was conducted on pore volume results of the paired methods. Three (3) statistical parameters were employed comprising the ratios $P_v/P_{LT}$, $P_I/P_v$, and $P_I/P_{LT}$; root mean square of errors (RMS) and coefficient of variation of errors (CVE). By definition, RMS = $\sqrt{(\mathrm{Residual})^2/\mathrm{N}}$, where *Residual* is the difference between corresponding porosity values of the paired methods, while N is the total number of paired data values. CVE is the ratio of RMS to mean of all paired data values, expressed as a percentage. It can be seen in Table 3 that mean values of the ratios $P_v/P_{LT}$, $P_I/P_v$ and $P_I/P_{LT}$ are 1.10, 1.18 and 1.28, respectively. The $Pv/P_{LT}$ ratio of 1.10 is quite close to 1.0, which indicates strong agreement between results of the VM and LTM. Considering the average values comprising $P_I/P_v$ = 1.18 and $P_I/P_{LT}$ = 1.28, it is evident that the IA method gives pore volume results that are about 20 to 30% higher than the corresponding values determined in accordance with the VM or LTM.

CVE values (Table 3) for the pairwise comparisons comprising ($P_v$, $P_{LT}$), ($P_v$, $P_I$) and ($P_{LT}$, $P_I$) are 19.9, 29.9 and 34.1%, respectively. Clearly, these observed CVE values fall within the range of 20 to 50%, which is the typical accuracy level of recognized prediction models (Bazant and Baweja, 1995; Ekolu, 2018; 2020).

Figure 10 shows residuals for pore volume results of the paired methods. Again, the pair ($P_v$, $P_{LT}$) shows the closest agreement of results, giving both the lowest CVE of 19.9% and a small spread of $\pm$5%. It is also evident in Fig. 10 that there was no heteroscedasticity such as fanning out or convergence of data points. Also plotted in Fig. 10 are the 95% confidence limits. It can be seen that the residuals for each pair of methods, all fall within the confidence limits. The foregoing statistical analysis thus shows that the three (3) porosity measurement methods comprising the VM, LTM and IA, may be employed interchangeably. However, the IA technique gives pore volume results that are 20 to 30% higher than corresponding values determined using the conventional methods.

Table 3
Statistical pairwise comparisons for pore volume results: Pv, $P_{LT}$ and $P_I$ are porosity values determined using the volumetric method (VM), linear – traverse method (LTM) and image analysis (IA), respectively.

| Sample ID | Pv (%) | $P_{LT}$ (%) | $P_I$ (%) | $Pv/P_{LT}$ ($Pv$, $P_{LT}$) | $P_I/Pv$ ($P_V$, $P_I$) | $P_I/P_{LT}$ ($P_{LT}$, $P_I$) |
|---|---|---|---|---|---|---|
| D6.7 | 15.0 | 18.45 | 15.2 | 0.81 | 1.01 | 0.82 |
| D9.5 | 22.7 | 15.76 | 21.8 | 1.44 | 0.96 | 1.38 |
| G6.7 | 23.4 | 23.99 | 32.1 | 0.98 | 1.37 | 1.34 |
| A9.5 | 27.1 | 22.14 | 18.9 | 1.22 | 0.70 | 0.85 |
| G9.5 | 17.9 | 18.45 | 26.3 | 0.97 | 1.47 | 1.43 |
| G9.5C | 21.1 | 15.76 | 30 | 1.34 | 1.42 | 1.90 |
| G13.2 | 22.6 | 29.19 | 34.5 | 0.77 | 1.53 | 1.18 |
| G13.2C | 30.6 | 27.42 | 35 | 1.12 | 1.14 | 1.28 |
| S6.7 | 26.7 | 21.92 | 36.2 | 1.22 | 1.36 | 1.65 |
| S6.7C | 23.3 | 21.06 | 19.5 | 1.10 | 0.84 | 0.93 |
| Mean | | | | 1.10 | 1.18 | 1.28 |
| RMS | | | | (4.4) | (7.5) | (8.2) |
| CVE (%) | | | | (19.9) | (29.9) | (34.1) |

## 3.2.4 Pore clogging effects

It was found as discussed in Sect. 3.2.1, that the conventional pore volume measurement methods comprising the VM and LTM, are unable to quantify pore clogging effects. However, other findings show that the falling head permeability test and IA technique, are able to effectively determine pore clogging effects in pervious concrete.

It can be seen in Fig. 11 that permeability results of the core specimens G9.5C, G13.2C, S6.7C reduced by 51.2, 16.8, 50.6% relative to corresponding values of control specimens G9.5, G13.2, S6.7, respectively. Evidently, pore clogging was responsible for the observed permeability reductions of nominally about 20 to 50%, depending on the type and size of aggregate used in pervious concrete.

IA results also showed that the pervious concrete samples (G9.5C, G13.2C, S6.7C) which had been used to treat AMD thereby giving rise to pore clogging, showed significantly smaller $d_c$ values relative to values of the corresponding control mixtures (G9.5, G13.2, S6.7) that were not exposed to AMD. For example, $d_c$ of the control specimen G9.5 reduced from 1.30 mm before pore clogging occurred to 0.90 mm after clogging in G9.5C, a significant decrease of 31%. Similarly, the 1.00 mm $d_c$ value of the control specimen G13.2 reduced by 35% to 0.65 mm of G13.2C.

## 3.2.5 Effects of aggregates on permeability results

Pervious concretes showed higher permeability with increase in size of the aggregate used, as seen in Fig. 11. For example, pervious concretes made with granite aggregate of various sizes comprising G6.7, G9.5 and G13.2, exhibited permeability values that correspondingly increased with increase in aggregate size, giving 5.6, 8.2 and 10.1 mm/s, respectively. Also, permeability results of pervious concretes made with the dolomite aggregate were significantly lower than corresponding values of the mixtures made with granite aggregate. For example, samples D6.7 /D9.5 gave permeability values of 0.9 /1.8 mm/s, which are 5 to 6 times less than the corresponding values comprising 5.6 /8.2 mm/s of samples G6.7 /G9.5, respectively. Pore volume results also showed a similar trend depicting this effect of the dolomite aggregate (Sect. 3.2.1). Of the various aggregate types used in the present study (Table 1), granite aggregate was found to be most suitable as it consistently gave the highest permeability results. Accordingly, a pervious concrete mixture prepared with granite aggregate expectedly exhibits a relatively more efficacious hydraulic conductivity. These observations also corroborate the earlier findings reported in Ekolu et al. (2016).

## 3.2.6 X - ray micro - computed tomography

X - ray microCT was employed for direct quantification of pore connectivity (Sect. 3.1.3). The total pore volume, connected porosity, isolated porosity and pore connectivity results of the samples G6.7 /G6.7FA, were determined to be 28.75 /19.10%, 28.65 /18.24%, 0.10 /0.86% and 99.7 /95.3%, respectively.

It is evident that incorporation of 30% FA into CEM I mixture (Sect. 2.1), altered the pore characteristics of pervious concrete, leading to reduction in pore connectivity from 99.7% for G6.7 to 95.3% for G6.7FA. This observed effect of FA on pore connectivity may partly be attributed to increase in paste volume of mixtures, owing to the relatively lower density of the supplementary cementitious material. More importantly, it is notable that the sample G6.7FA gave a significantly higher isolated porosity of 0.86%, compared to the much smaller 0.10% value of G6.7. The higher isolated porosity of G6.7FA is directly attributed to discrete pore blockages typically resulting from incorporation of FA into concrete mixtures. It is the implied presence of FA – induced discrete pore blockages, that majorly accounts for the significantly reduced pore connectivity of sample G6.7FA.

Figure 12 gives microCT slice 2D images of the core samples G6.7 and G6.7FA. The black features seen within sample geometry are the irregular - shaped pores, while the dark gray irregular shaped features are aggregate particles. The surface – coating seen on aggregate particles is hardened paste, while the bright dotted spots in the paste are alite particles of unhydrated or partially hydrated cement grains. The slice microCT images of G6.7 (Fig. 12a,b) and of G6.7FA(Fig. 12c,d), both show high pore connectivity levels, consistent with the measured values comprising 99.7 and 95.3%, respectively.

## 4. Conclusions

While pervious concrete is effective as a permeable reactive barrier for treatment of acid mine drainage (AMD), pore clogging also occurs simultaneously. In the foregone study, pervious concrete effectively removed 90 to 99% of the various heavy metals comprising Al, Fe, Zn, Mn and Mg. However, Cr concentration increased significantly in the treated AMD effluent, owing to leaching of the hazardous element from Portland cement and fly ash materials used in pervious concrete mixtures.

The study also evaluated pore volume, connectivity and clogging of pervious concretes made with aggregates of different types and sizes. Five different methods were used to conduct evaluations; they comprise:- the volumetric method (VM), linear – traverse method (LTM), image analysis (IA), falling head permeability test and X – ray micro – computed tomography (microCT).

Statistical analysis showed that pore volume measurement methods consisting of the VM, LTM and IA, may be employed interchangeably. The VM and LTM gave similar pore volume results, while IA's values were consistently 20 to 30% higher than results determined using the conventional methods.

The falling head permeability test and IA technique, were found to be effective methods of quantifying pore clogging effects in pervious concrete. Pore connectivity of pervious concrete was found to be very high, being 95.0 to 99.7% as determined using microCT. Nonetheless, isolated porosity increased while pore connectivity reduced in pervious concretes containing fly ash. The observed high pore connectivity underlies the efficacious hydraulic conductivity of pervious concrete as a permeable reactive barrier for AMD treatment.

# Declarations

### Conflict of Interest

The authors declare no conflict of interest.

### Ethics Approval and Consent to Participate

Not applicable.

### Consent to Participate

Not applicable.

### Availability of Data and Materials

All data generated and analysed during this study are included in this published article.


### Funding

No funding source to declare.


### Competing Interests

The authors declare no competing interests.

### Authors Contributions

SOE conceptualised the research and drafted the manuscript, FS prepared experimental set-ups and supervision of tests, FCdB conducted microCT tomography, LB conducted column studies, RNK conducted image analysis, KTM and FGM conducted porosity measurements.

# References

1. ASTM C1754 (2012), Standard test method for density and void content of hardened pervious concrete, *ASTM International*, West Conshohocken, PA, 2012, www.astm.org
2. ASTM C457 (2016), Standard test method for microscopical determination of parameters of the air-void system in hardened concrete, *ASTM International*, West Conshohocken, PA, 2016, www.astm.org
3. Bartzas G. and Komnitsas K. (2010), Solid phase studies and geochemical modelling of low-cost permeable reactive barriers, *Journal of Hazardous Materials* 183 (1-3), 301-308.
4. Bazant Z.P and Baweja S (1995), Justification and refinements of Model B3 for concrete creep and shrinkage, 1. Statistics and sensitivity, *Materials and Structures*, 28, 415-430.
5. Brown H.J. (2013), Monitoring pervious concrete for water quality in a laboratory and field environment, *Concrete Industry Management* (presentation, 62 slides), http://www.rmcfoundation.org/ (accessed 28/05/2013).
6. Collins, K., Hunt, W. and Hathaway, J. (2008), Hydrologic comparison of four types of permeable pavement and standard asphalt in Eastern North Carolina, *Journal of Hydrologic Engineering*, 13(12), 1146-1157.
7. Das B.M. (1998), *Principles of Geotechnical Engineering*, 4th Ed.., PWS Publishing Co., Massachusetts, USA.
8. Diamond S. and Leeman M.E. (1995), Pore size distributions in hardened cement paste by SEM image analysis, *Materials Research Society Symposium*, Vol. 370, 217 – 226.
9. du Plessis A. and Boshoff W.P. (2019), A review of X-ray computed tomography of concrete and asphalt construction materials, *Construction and Building Materials* 199, 637–651.
10. Ekolu S.O. (2018), Model for practical prediction of natural carbonation in reinforced concrete: Part 1-formulation, *Cement and Concrete Composites* 86, 40-56.
11. Ekolu S.O. (2020), Model for natural carbonation prediction (NCP): practical application worldwide to real life functioning concrete structures, *Engineering Structures*, Vol. 224, 1 December, 111126.
12. Ekolu S.O. and Bitandi L.K. (2018), Prediction of longevities of ZVI and pervious concrete reactive barriers using the transport simulation model, ASCE, *Journal of Environmental Engineering*, 144(9): 04018074.
13. Ekolu S.O., Azene F.Z. and Diop S. (2014), A concrete reactive barrier for acid mine drainage treatment, *Proc. Inst. Civil Eng. Water Manag*. 167 373–380.
14. Ekolu S.O., Diop S. and Azene F. (2016), Properties of pervious concrete for hydrological applications, *Concrete Beton*, 144, March, 18-25.
15. Eshel G., Levy G., Mingelgrin U. and Singer M. (2004), Critical evaluation of the use of laser diffraction for particle-size distribution analysis, *Soil Science Society of America Journal*, 68(3), 736-743.
16. Ferreira T. and Rasband W. (2012), *ImageJ User Guide*, guide IJ 1.46r, 198p, https://imagej.nih.gov/ij/docs/guide/user-guide.pdf
17. Gavaskar A. (1999), Design and construction techniques for permeable reactive barriers, *Journal of Hazardous Materials* 68(1–2), 41-71.
18. Gavaskar A., Sass B., Gupta N., Hicks J., Yoon S., Fox T. and Sminchak J. (1998), *Performance evaluation of a pilot-scale permeable reactive barrier at former Naval Air Station Moffett Field*, Mountain View, California. Final report prepared by Battelle, Columbus, Ohio for Naval Facilities, Engineering Service Center, Port Hueneme, CA. Project Sponsored by ESTCP, 191p.
19. Holmes R.R., Hart M.L. and Kevern J.T. (2017), Heavy metal removal capacity of individual components of permeable reactive concrete, *Journal of Contaminant Hydrology* 196, 52-61.
20. Kevern J.T, Kejin W. and Schaefer V.R. (2008), Pervious concrete in severe exposures - development of pollution-reducing pavements for Northern cities, *Concrete International*, 43-49.
21. Kia A., Wong H.S. and Cheeseman C.R. (2017), Clogging in permeable concrete: a review, *Journal of Environmental Management* 193 (2017) 221-233.
22. Lucke T. and Beecham S. (2011), Field investigation of clogging in a permeable pavement system, *Journal of Building Research and Information*, Routledge, 39(6), pp. 603-615.

23. Majersky G. (2009), *Metals recovery from acid mine drainage using pervious concrete*, VDM Publishing House, ISBN 978-3-639-02618-4, paperback, 69p.
24. Montes F., Valavala S. and Haselbach M. (2005), A new test method for porosity measurements of Portland cement pervious concrete, *Journal of ASTM International*, 2 (1), 1–13.
25. Morrison S.J, Naftz D.L, Davis J.A. and Fuller C.C. (2003), Chapter 1 - Introduction to groundwater remediation of metals, radionuclides, and nutrients with permeable reactive barriers, *Handbook of Groundwater Remediation using Permeable Reactive Barriers*, 1-15. http://0-www.sciencedirect.com/
26. Mulligan C.N., Yong R.N. and Gibbs B.F. (2001), Remediation technologies for metal-contaminated soils and groundwater: an evaluation, *Engineering Geology* 60 (1–4), 193-207.
27. Muthu M., Santhanam M. and Kumar M (2018), Pb removal in pervious concrete filter: Effects of accelerated carbonation and hydraulic retention time, *Construction and Building Materials* 174 (2018) 224–232.
28. Neithalath N., Sumanasooriya M.S. and Deo O. (2010), Characterizing pore volume, sizes, and connectivity in pervious concretes for permeability prediction, *Materials Characterisation* 61, 802 – 813.
29. Obiri-Nyarko F., Grajales-Mesa S.J. and Malina G. (2014), An overview of permeable reactive barriers for in situ sustainable groundwater remediation, *Chemosphere* 111, 243-259.
30. Ong S.K, Wang K., Ling Y. and Shi G. (2016), *Pervious concrete physical characteristics and effectiveness in stormwater pollution reduction*, Iowa State University, Institute of Transportation, Final Report, April 2016, 57p.
31. Pagotto C., Legret M. and Le Cloirec P. (2000), Comparison of the hydraulic behaviour and the quality of highway run-off water according to the type of pavement, *Water Research* 34 (18), 4446-4454.
32. Park S-B. and Tia M. (2004), An experimental study on water purification properties of porous concrete, *Cement and Concrete Research* 34, 177-184.
33. Potgieter, S.S., Panichev, N., Potgieter, J.H. and Panicheva, S. (2003), Determination of hexavalent chromium in South African cements and cement-related materials with electrothermal atomic absorption spectrometry, *Cement and Concrete Research,* 33 (10), 1589–1593.
34. Pratt C.J., Mantle J.D.G., and Scholfield P.A. (1995), UK research into the performance of permeable pavement, reservoir structures in controlling stormwater discharge quantity and quality, *Water Science and Technology* 32 (1), 63-69.
35. Radlinska A., Welker A., Greising K., Campbell B. and Littlewood D. (2012), Long-term field performance of pervious concrete, *Advances in Civil Engineering*, Hindawi, Article ID 380795, https://doi.org/10.1155/2012/380795
36. Sañudo-Fontaneda L.A, Charlesworth S.M, Castro-Fresno D., Andrés-Valeri V.C.A. and Rodriguez-Hernandez J. (2014), Water quality and quantity assessment of pervious pavements performance in experimental car park areas, *Water Science and Technology* 69 (7), 1526-1533.
37. Sawyer T. (2012), Assessment of the suitability of ground granulated arc furnace slag as a cementitious extender, *Technical Report*, 14p., accessed on 27 December 2019, at https://www.researchgate.net/publication/318490127
38. Tennis P.D., Leming M.L. and Akers D.J. (2004), *Pervious concrete pavements*, EB302.02, Portland Cement Association, Skokie, Illinois, and National Ready Mixed Concrete Association, Maryland, USA, 2004, 36p.
39. Thiruvenkatachari R., Vigneswaran S. and Naidu R. (2008), Permeable reactive barrier for groundwater remediation. *Journal of Industrial and Engineering Chemistry* 14, 145–156.
40. Zhong R., Leng Z. and Poon C-S (2018), Research and application of pervious concrete as a sustainable pavement material: a state-of-the-art and state-of-the-practice review, *Construction and Building Materials* 183, 544–553.

# Figures

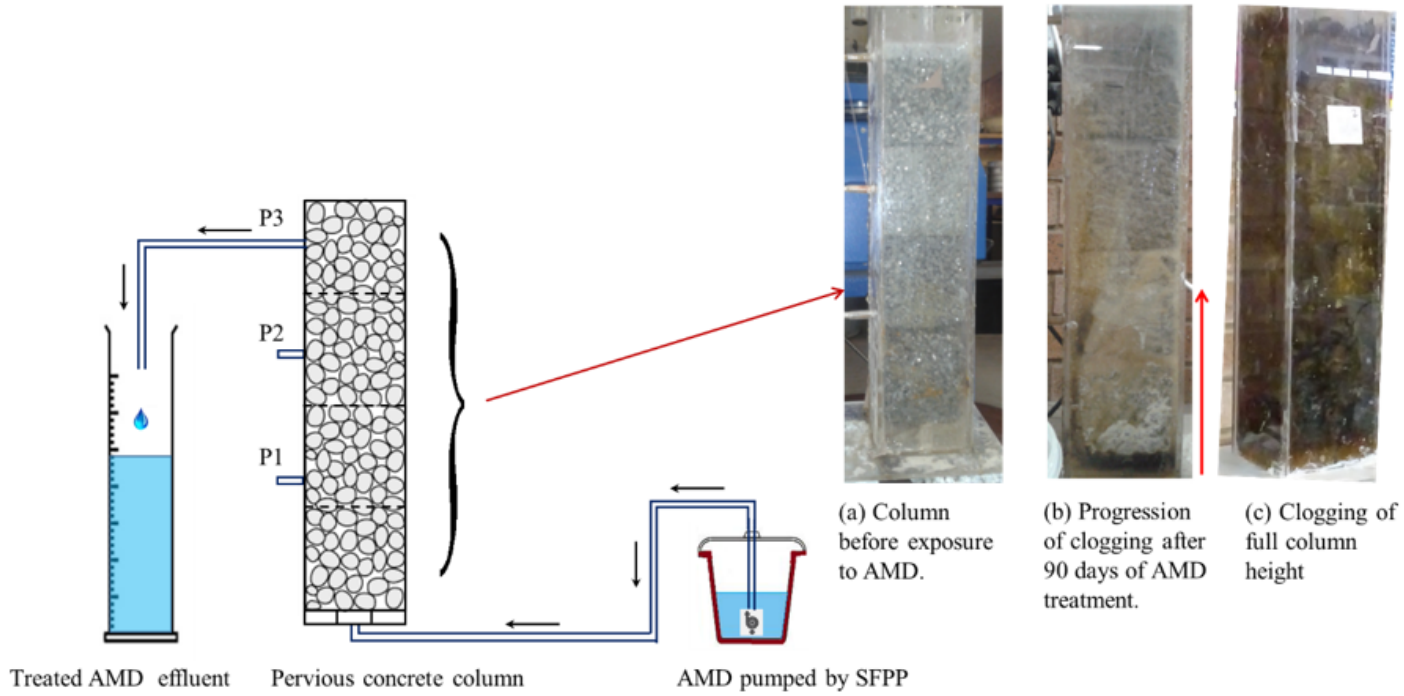


**Figure 1**

Pervious concrete column set - up (a) before exposure to acid mine drainage (AMD), (b) progression of clogging following 90 days of AMD treatment, (c) clogging of full column height (adapted from Ekolu and Bitandi, 2018).

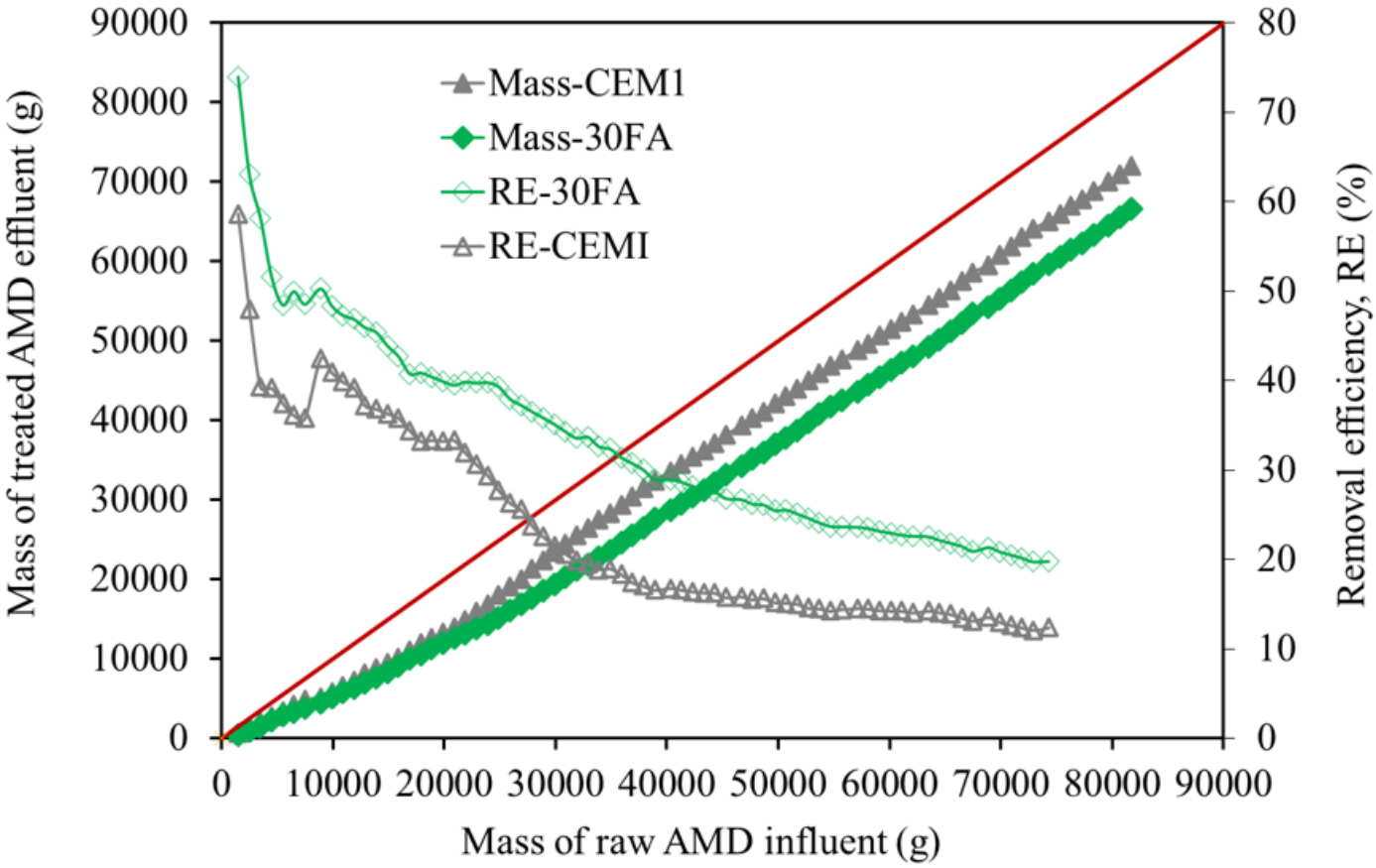

**Figure 2**

Cumulative mass values of acid mine drainage (AMD) influent versus effluent, along with contaminant removal efficiency (RE): Mass-CEMI is graph of cumulative mass values for CEM I - pervious concrete; RE-30FA is graph of RE for 30FA - pervious concrete etc.


**Figure 3**

Pervious concrete samples (a) 100 mm cubes, (b) 70 dia. x 100 mm thick cores, (d) 70 dia. x 35 mm thick disc specimens.

**Figure 4**

Disc specimens of 70 dia. x 35 mm thickness showing traversing lines spaced at 2.5 mm.

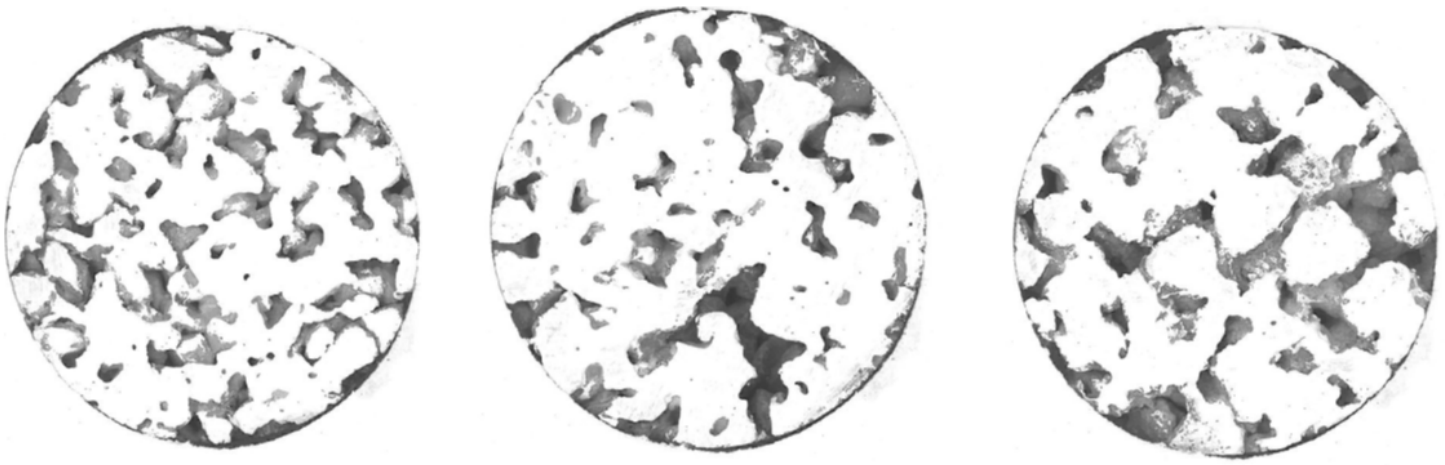

**Figure 5**

Scanned images of 70 dia. x 35 mm thick disc specimens.

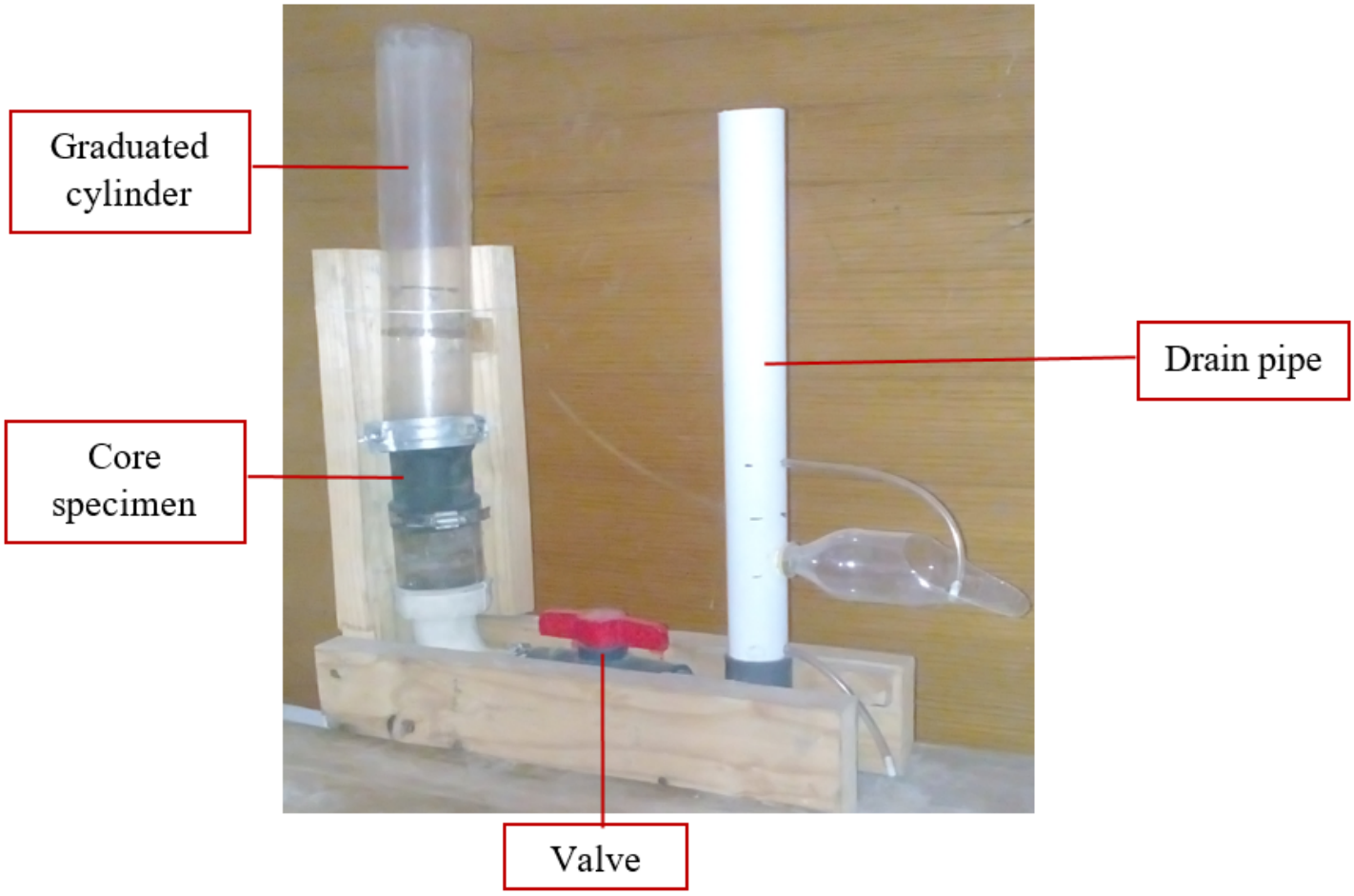


**Figure 6**

Falling head permeameter.

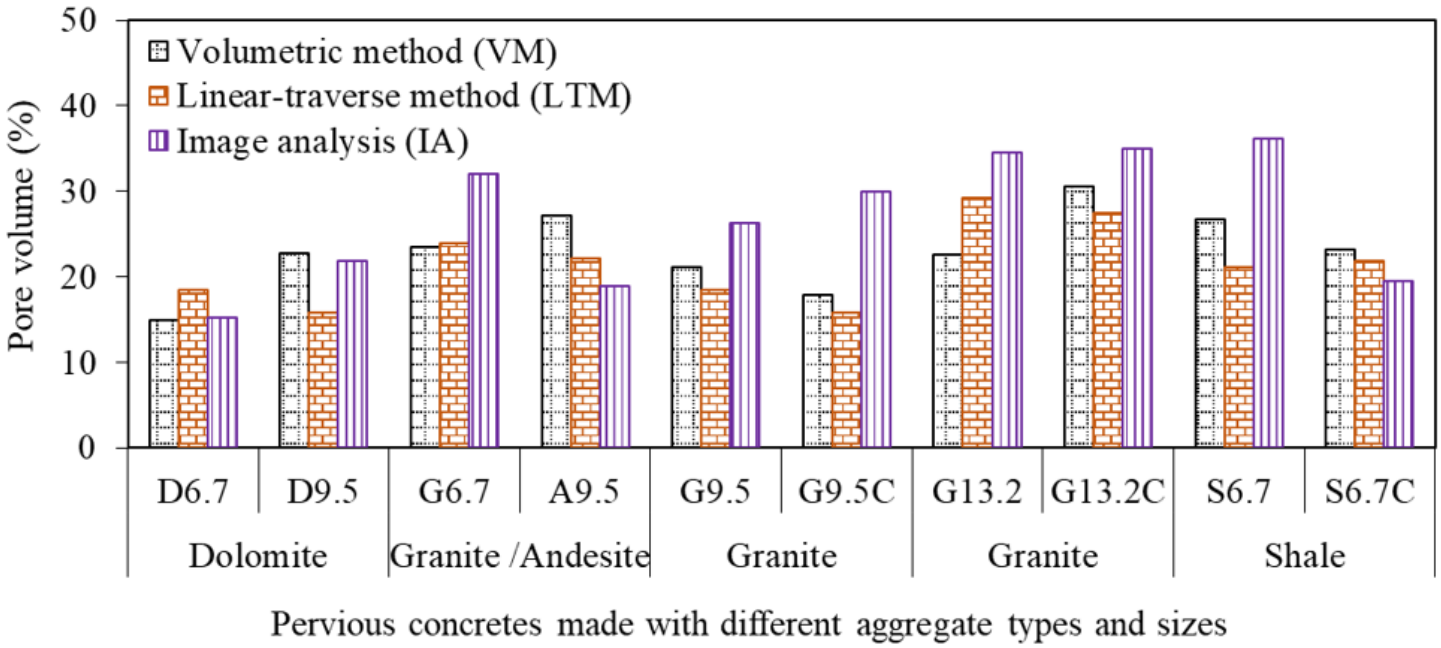


**Figure 7**

Pore volume results determined using the volumetric method (VM), linear – traverse method (LTM) and image analysis (IA).

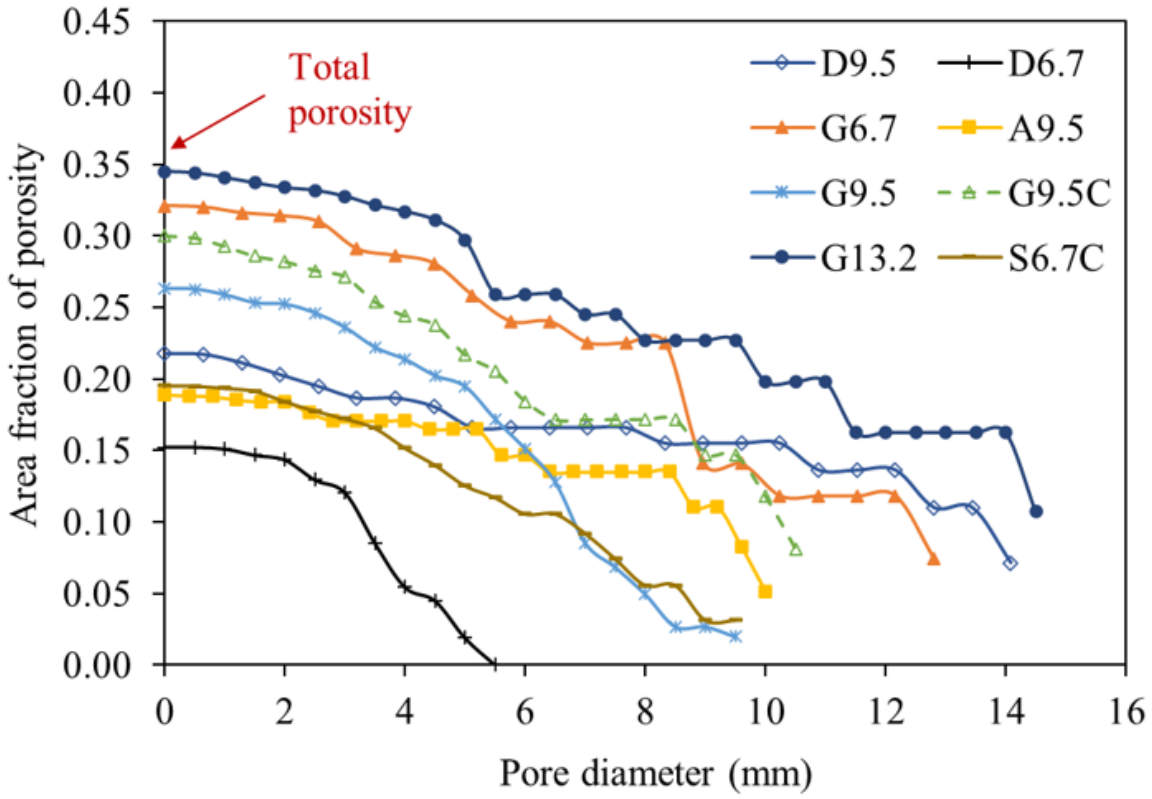


**Figure 8**

Pore size distributions determined using image analysis.

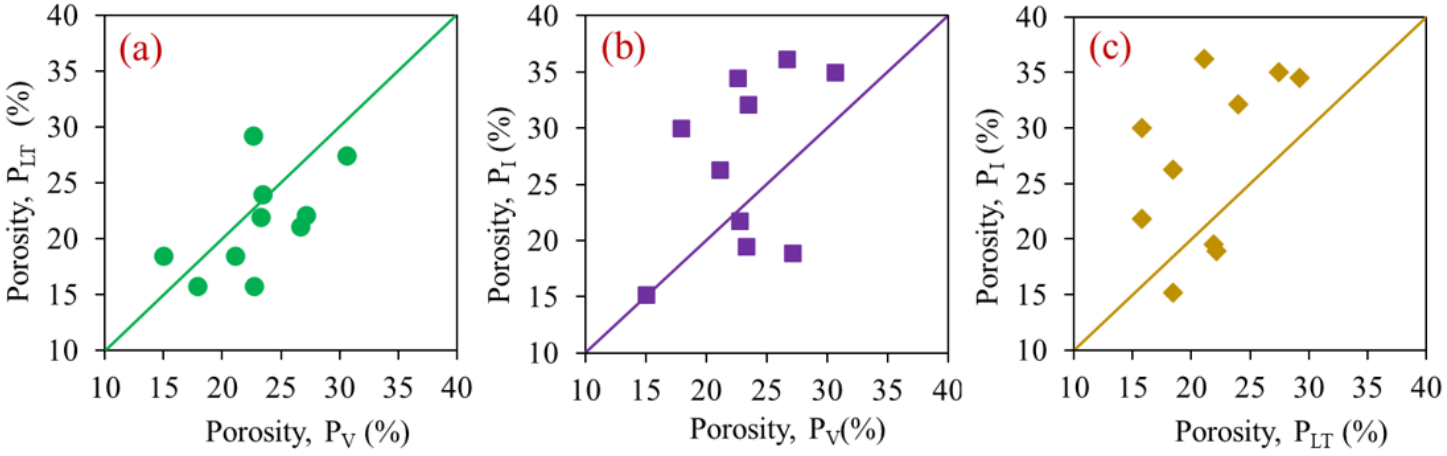


**Figure 9**

Pairwise comparisons for pore volume values Pv, PLT and PI determined using the volumetric method (VM), linear – traverse method (LTM) and image analysis (IA), respectively.

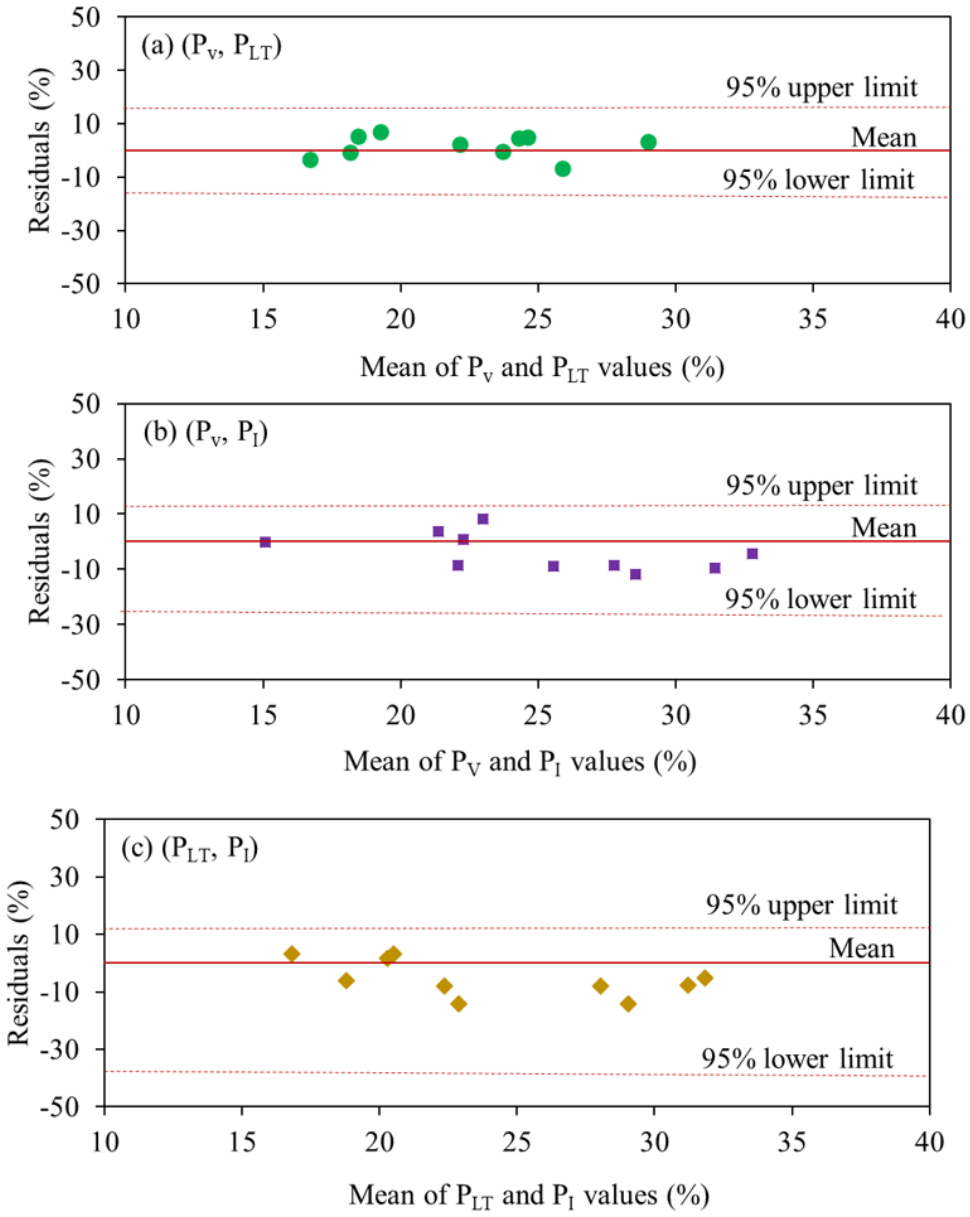


**Figure 10**

Residuals of pore volume results of the paired methods (a) (Pv, PLT), (b) (PV, PI), (c) (PLT, PI); where Pv, PLT and PI are porosity values determined using the volumetric method (VM), linear – traverse method (LTM) and image analysis (IA), respectively.

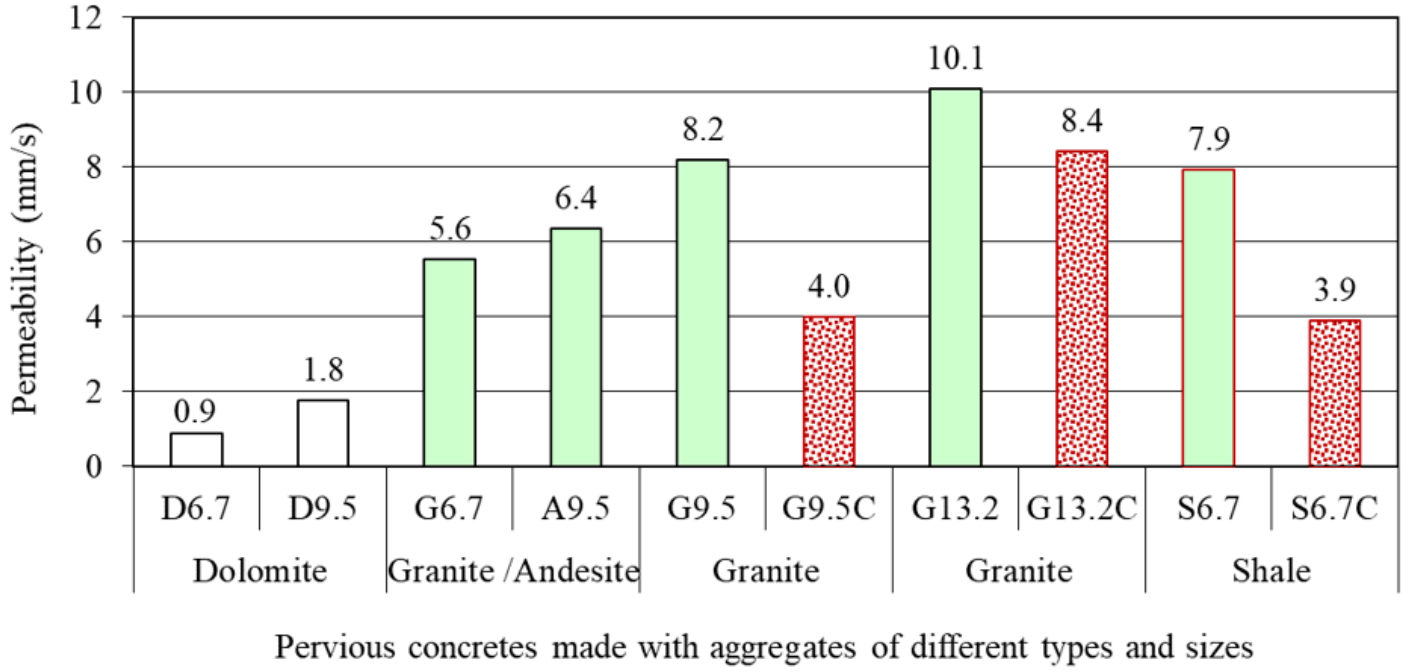


Figure 11

Permeability results showing the effects of pore clogging, aggregate types and sizes.

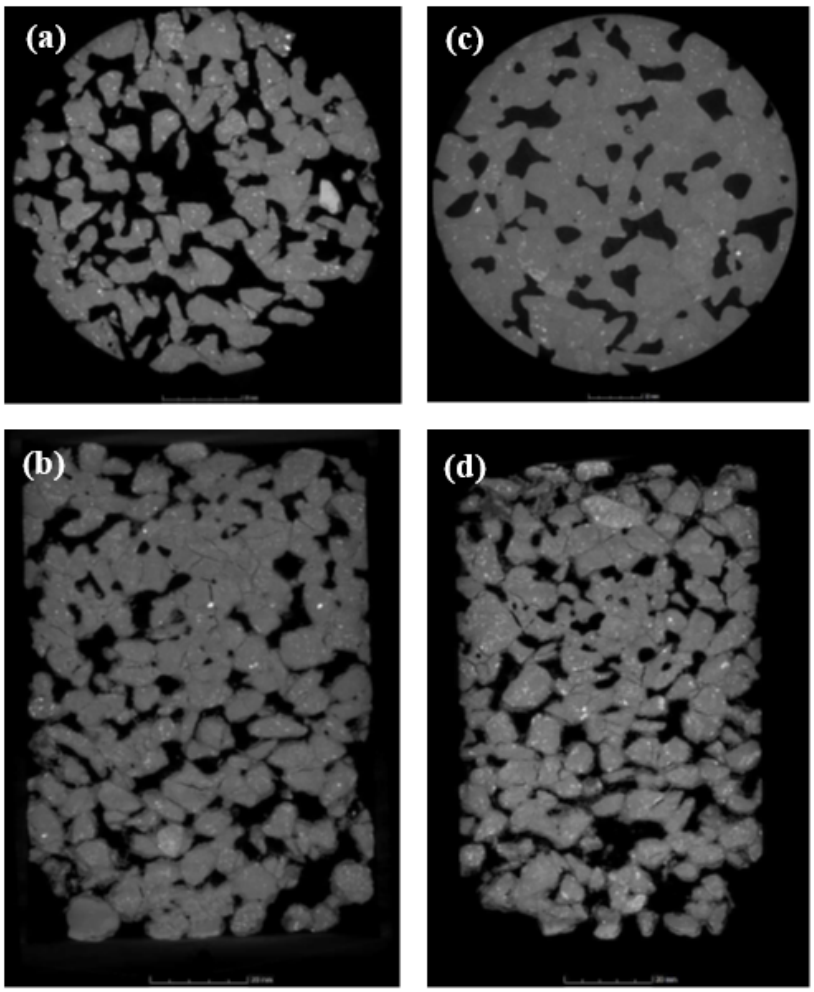


Figure 12

MicroCT slice 2D images of 70 dia. x 100 mm thick pervious concrete cores: (a,b) cross - sectional and vertical slices of sample G6.7, (c,d) cross – sectional and vertical slices of sample G6.7FA.